Reworkable Die-to-Wafer Hybrid Bonding Process

Rajan Gangadharan
Adeia Inc
San Jose, USA
rajan.gangadharan@adeia.com

Dominik Suwito
Adeia Inc
San Jose, USA
dominik.suwito@adeia.com

Thomas Workman
Adeia Inc
San Jose, USA
thomas.workman@adeia.com

Cyprian Uzoh
Adeia Inc
San Jose, USA
cyprian.uzoh@adeia.com

Justin Chen
Adeia Inc
San Jose, USA
justin.chen@adeia.com

Pawel Mrozek
Adeia Inc
Morrisville, USA
pawel.mrozek@adeia.com

Arianna Avellan
Adeia Inc
San Jose, USA
arianna.avellan@adeia.com

Suhail Sadiq
Adeia Inc
San Jose, USA
suhail.sadiq@adeia.com

Laura Mirkarimi
Adeia Inc
San Jose, USA
laura.mirkarimi@adeia.com

***Abstract*— Hybrid bonding enables finer interconnect pitch than micro-bumps and with improved electrical/thermal performance and reliability, but die-to-wafer (D2W) hybrid bonding lacks an established rework capability. For assemblies with multiple hybrid bonded dies, a rework process is highly desirable to prevent scrapping parts because of a single failed bond. This work presents practical D2W rework methods that can remove standard hybrid bonded dies when defects are detected before post-bond anneal, and successfully rebond to those sites. Rework disposition will be driven by optical inspection for voids and misalignment. Two die removal techniques are evaluated: (1) blade-based die removal, and (2) a pull-based method which removes the die by lifting the die with a stud adhesively attached to the die backside. Successful die removal is demonstrated for die sizes from 3×3 mm to 26×32 mm and die thicknesses of 50 µm, 200 µm, and 450 µm.**

Debonding was possible with reasonably low debond forces up to 7 days after bonding with room temperature storage. To enable debonding after longer delays, low temperature storage (<0ºC) kept die bond energy low enough to enable debonding after more than a month.

Verification of functionality of rebonded material was performed on 8×12 mm, 200 µm thick daisy-chain test vehicles (~32k links). Dies were debonded successfully with a force of approximately 1 kgf. The electrical yield of rebonded sites for both pull and blade removal methods was 90–95%, matching the first-bond yield.

The low force debond is achieved by initiating a debond front that propagates from one die edge across the entire die surface. In the methods used, debond force remained relatively constant with die thickness and increased minimally with increasing die size.

The methods used are suitable, with refinements, for a high-volume manufacturable debond and rework process.

Keywords*— *Cu to Cu direct bonding, direct bond interconnect (DBI), Hybrid bonding, Die to Wafer (D2W) Hybrid bonding, D2W debonding, D2W rework, D2W repair

I. Introduction

Hybrid bonding offers clear advantages over micro-bumps: it supports finer pitch with better electrical and thermal properties and has superior reliability. Yet, unlike micro-bumps and wafer-to-wafer hybrid bonding (W2W) [1], there is still no established die-to-wafer hybrid bonding (D2W) rework process [2 - 4]. Significant demand for a rework process in hybrid bonding assembly processes exists because the industry is adopting this technology for high-end advanced packaging applications. This paper describes practical methods to rework D2W hybrid bonded structures.

In the hybrid bonding process, bondable surfaces are prepared to be very flat and to have a controlled copper recess using chemical mechanical polishing (CMP). The surfaces are then plasma activated and hydrated to form Si–OH and Si-N-OH groups that enhance hydrophilic bonding. Bonding is performed at room temperature by bringing the two surfaces into direct contact. A subsequent anneal joins the Cu interconnects and condenses interfacial Si–OH and Si-N-OH into covalent Si–O–Si (siloxane) and Si-N-Si-O bonds, which raises the bond energy of the dielectric-dielectric interface. These higher post-anneal bond energies—especially the Cu–Cu connection—make separation and rework infeasible. Accordingly, our die removal trials focus on the pre-anneal state, when the interface is mainly held by hydrogen bonds and bond energies are low. While electrical testing cannot be performed before Cu interconnects are formed, optical inspection is well suited to find bond voids and alignment issues, both indicators for rework.

A practical rework flow must remove the die without damage to the die or substrate bond site and neighboring areas or cause particulate contamination that cannot be effectively removed. This will allow debonded sites to be repopulated and debonded die to be reused after a suitable cleaning process. The dielectric surface properties and metal interconnect recess of the reworked material must be returned to a bondable condition after completion of the debonding and cleaning steps.

In this paper, we evaluate two removal techniques (blade- and pull-based) that removed bonded die from a substrate and allowed fresh die to be successfully bonded in their place without defect. Reuse of debonded dies after a suitable clean will be addressed in future work.

II. Experimental Procedure

A. Test Vehicles

Assemblies of TOx dies (silicon die with thermally oxidized bond surface) bonded to 200 mm TOx wafers (silicon wafer with thermally oxidized bond surface) were used as the experimental test vehicle to perform pull-force and bond void studies. No additional CMP was performed on the TOx wafers since the topography of the originally mirror-polished silicon wafers meets bonding specifications. Both mechanical saw dicing and stealth dicing were used for singulation of the TOx dies. The debonding trials included multiple die thicknesses (50 µm, 200 µm, and 450 µm) and die footprints (3×3 mm, 3.5×5.2 mm, 8×12 mm, and 26×32 mm) to quantify removal forces and identify thickness and size dependencies.

To assess the impact of "rework" (die removal and bonding of "fresh" die onto same bond site) on the electrical properties of hybrid bonded structures, we used an electrical test vehicle featuring 10 µm DBI Cu pads on 40 µm pitch. The DBI layer and redistribution layer (RDL) underneath were formed by sequential single damascene Cu metallization in silicon dioxide. Various daisy chain arrays allow for the electrical testing of the interconnect quality post bond and anneal (Fig. 1). Reported electrical yield and chain resistances refer to the longest chain in the center of the die (DC) with ~32k interconnects as well as to the bottom edge chain (DCT2) with ~3.5k interconnects. The edge chain gets as close as 260 µm to the physical edge of the die and is therefore sensitive to potential edge defects. The die size for the electrical test vehicle is 8x12 mm, and the die thickness is 200 µm.

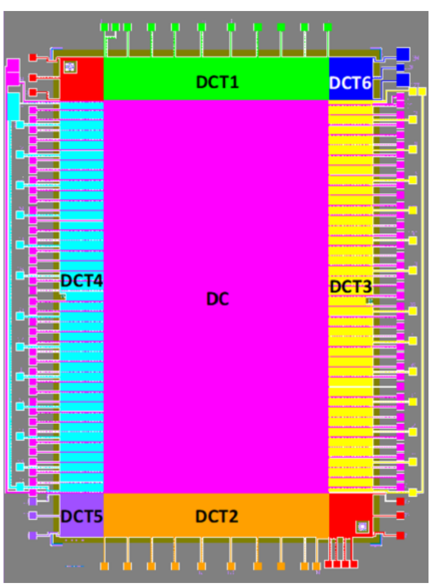

Fig. 1 Daisy chain layout for electrical test vehicle

For the electrical test vehicle, CMP was performed to achieve the specified dielectric flatness and metal recess on both die and substrate. Singulation of the dies was performed by stealth dicing.

B. Surface preparation and bonding process

After cleaning, surfaces were plasma activated and hydrated to form hydrophilic Si–OH termination. The dies were then bonded to the substrate wafers in a Besi Datacon 8800 CHAMEO advanced bonder with an ISO 3 clean kit (alignment accuracy is 3 µm 3 σ). The bonding was performed with minimal bond force. The final die and substrate cleaning, activation, bonding, and anneal were performed in Adeia's prototyping laboratory in a Class 1000 cleanroom. These process steps describe Adeia's standard pre-bond preparation and bonding without any modification to reduce bond energy or aid in the debond process.

C. Debond trials

Since the post-bond anneal forms Cu–Cu connections and condenses interfacial silanol into siloxane (Si–O–Si), debond trials were performed in the pre-anneal condition where the interface is mainly hydrogen-bonded with low bond energies. For this pre-anneal state, optical inspection (voids/alignment) is the primary metrology to screen for the necessity of rework since electrical testing is not yet possible. The debonded sites in these trials were selected in a contiguous area of the substrate without regard to whether or not defects (voids or misalignment) were present on any of the debonded sites.

1. Blade-based die removal

Two different die-removal techniques were explored. In the first approach, a custom tool was used to engage a blade against the edge of the die to be removed (Fig. 2). The blade was positioned on the die edge as near as possible to the substrate surface, then pressed to frictionally engage and lift the die with a predominantly upward motion and slight rotation. (See schematic of the blade-based removal technique in Fig. 3.) This approach avoids inserting the blade between die and substrate and is designed to prevent blade contact with the substrate surface. A vacuum catcher placed immediately above the die captured the die immediately after lift.

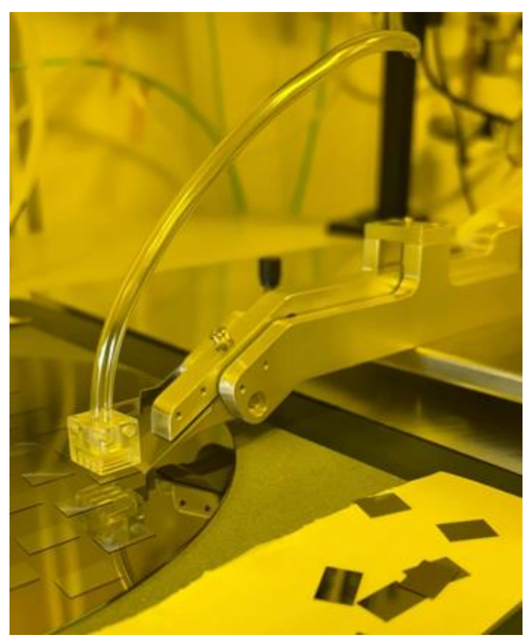

Fig. 2 Custom tool used for blade-based die removal

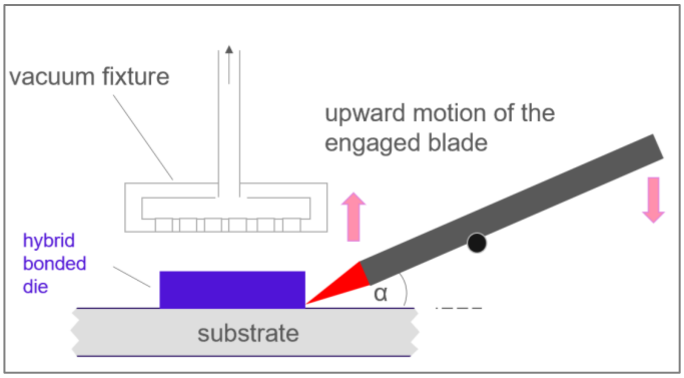

Fig. 3 Schematic of the blade-based die removal technique

2. *Adhesive-based stud pull approach*

In the second approach, metal studs were adhesively attached to the die backside. Dies were then removed by pulling the stud straight upward. Initial evaluation used manual pulling which introduced lateral/rolling motion and, as a consequence, handling damage (scratches and debris at die edges). Therefore, all trials were performed using a machine-based straight upward pull to minimize lateral motion and handling damage. Fig. 4 shows the XYZTec Condor Sigma pull tester used and Fig. 5 shows a schematic of the adhesive-based die removal technique. The pull tester allows for measuring the pull force as a function of pull head displacement and time. During the pull, the wafers were held on a vacuum stage and the studs were pulled up at a constant rate of 100 µm/s. The peak force needed to remove the dies was derived from the force displacement curves.

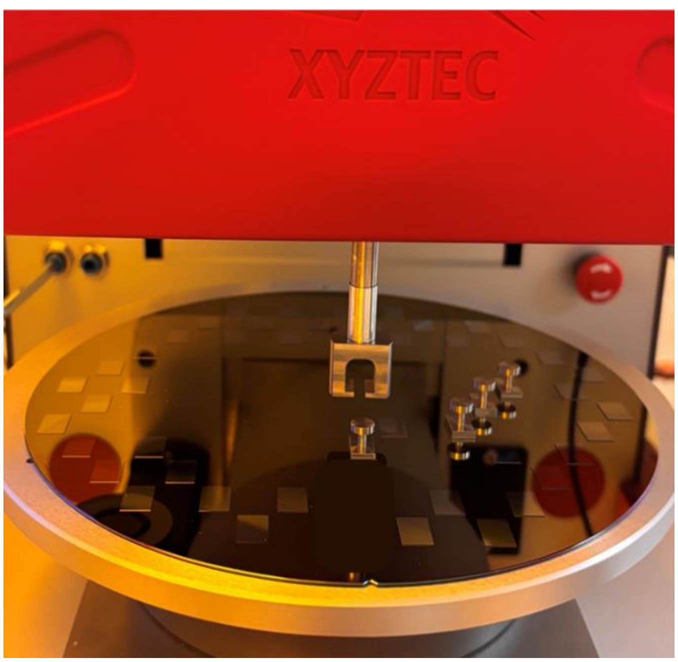

Fig. 4 XYZTec Condor Sigma pull tester used for adhesive-based die removal technique

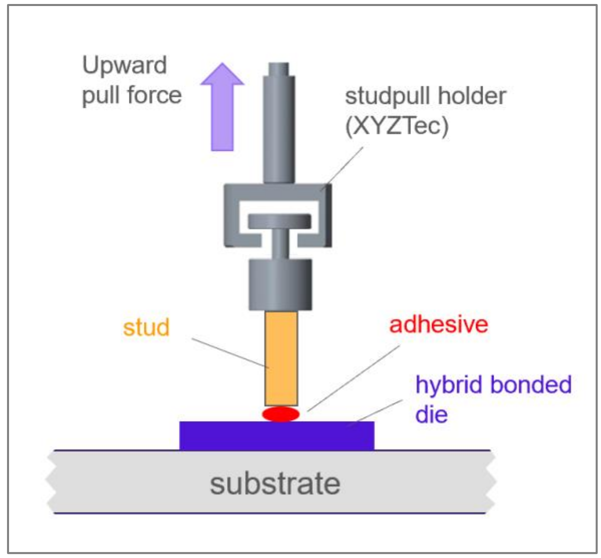

Fig. 5 Schematic of the adhesive-based die removal technique

D. Rebond and electrical test

Initial tests showed that an efficient substrate cleaning process was required after die removal because particles generated from handling and die removal were difficult to remove with a standard cleaning process. Therefore, a high-pressure cleaning process (HPC) with alkaline and surfactant chemistry was developed to efficiently remove particles after the de-bonding process [5]. After the clean, the substrate wafers were re-activated with plasma treatment.

For the electrical tests, the first round of bonding was performed on roughly 70% of the sites. Two-third of these sites were debonded within 24 hours. The remaining bonded sites are called *first round bond sites*. After cleaning, a second round of bonding was performed. In this second round of bonding, all the debonded sites were rebonded with fresh dies. This group is called *rebond sites*. An additional group of dies was bonded in the second round to sites that had not before been bonded but were near debonded sites. This group is called *second round bond sites*. The yield of these 3 groups was compared to assess the effect of debonding on the debonded sites and neighboring areas.

After the second round of bonding was completed, an anneal at 300˚C was performed to form the Cu-Cu interconnects to enable electrical testing.

E. Metrology and inspection

Bond quality (bond voids) was evaluated by an optical inspection method and C-mode scanning acoustic microscopy (CSAM). In addition, Surfscan was used to assess surface cleanliness of the substrate after die de-bond and after clean, and IR inspection was performed for defect type identification. Surface topography (dielectric roughness and Cu recess) before and after debond was measured by AFM. Electrical performance was assessed using daisy-chain continuity and resistance measurements on the patterned test structures across multiple chain regions.

III. Results

A. Die removal versus queue time and storage temperature

With bonded samples kept at room temperature, the debonding was successful with a delay time up to at least 7 days after bonding. Low-temperature storage was explored as a means to allow longer delays between bonding and debonding on 200 µm thick 8x12 mm dies. Bonded wafers were stored at the refrigeration temperature for a period of days, allowed to warm to room temperature to perform pull testing on a subset of bonded die, then returned to refrigeration temperature until the next pull test. With −20°C storage, die removal was achieved with only a moderate increase in pull force even after 32 days. The pull-force evolution versus time is shown in Fig. 6.

To confirm that these trends are linked to bond-energy (BE) increase with storage time, BE measurements were performed on bonded wafer-to-wafer (W2W) pairs based on the Maszara methodology [6]. We direct bonded pairs of 300 mm TOx wafers to benchmark how post-bond storage temperature affects bond energy, and to interpret the die-to-wafer (D2W) debond behavior. The pre-clean and activation processes for these wafers was identical to the processes used for the D2W bonding. The W2W time-series results (Fig. 7) show that room-temperature storage produced a strong BE increase with time, while cooler storage temperatures suppressed this increase. Importantly, after storage, a subsequent 150°C / 15 min anneal resulted in similarly high BEs (~3000 mJ/m²) irrespective of the storage history, indicating that low-temperature storage mainly delays interfacial strengthening. This W2W evidence supports the D2W observations: the "easy removal" after weeks is consistent with suppressed self-annealing during cold storage, and the low BE quantified in W2W provides the mechanistic basis for the persistently debondable condition observed in D2W bonded samples after ~1 month.

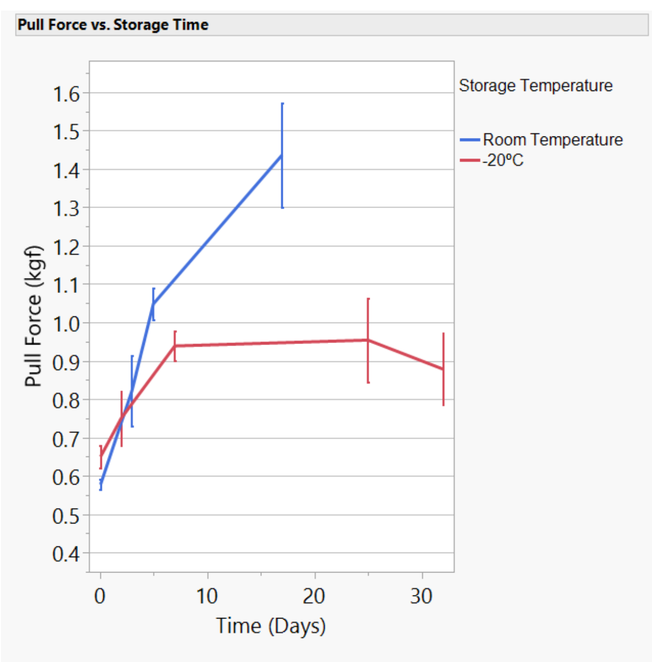

Fig. 6 D2W pull force increase with time at -20°C and room temperature storage

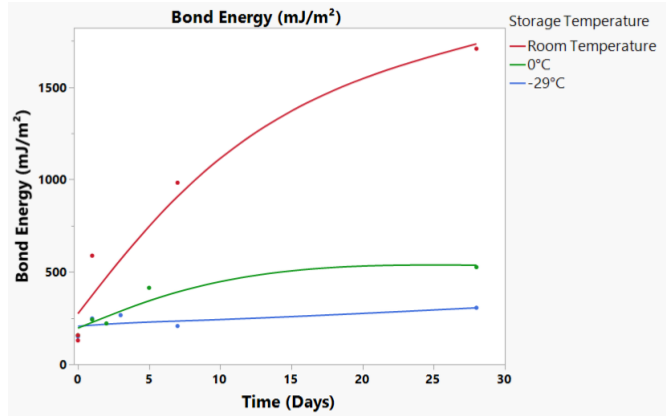

Fig. 7 W2W bond energy increase with time at different storage temperatures

B. AFM studies of electric test vehicle

AFM measurements on electric test vehicle substrates indicate that the debond process does not change the topography of the debonded surfaces, neither for the pull-based die removal nor for the blade-based method. Dielectric surface roughness and Cu recess before and after de-bonding are essentially the same (Fig. 8).

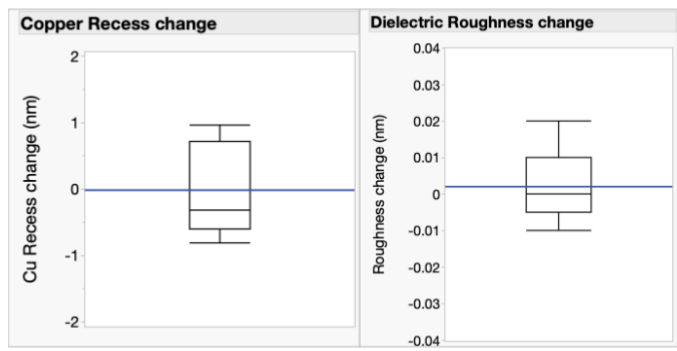

Fig. 8 AFM Results on Substrate wafer (difference between before bonding and after debonding)

C. Debond/Rebond with Blade-based die removal method

To evaluate the debond/rebond process, the success criteria are that the rebonded sites are void free and that all daisy chains of the electrical test vehicle pass electrical connectivity and show resistances close to the theoretical value.

Using the electrical test vehicle together with the blade-based die removal method and the HPC clean/re-activation sequence described earlier, the rebond sites achieved a 97% electrical yield on the main daisy-chain (DC), compared to 88% for the first and second time-bond sites (Table 1). Fig. 9 shows similar main-chain resistance at the rebonded site and the first and second round bond sites, indicating that the die removal using the blade-based method and rebonding process does not affect interconnect continuity. The observed electric yield loss is consistent with bond voiding, as indicated by the CSAM results in Fig. 10. The relatively low yield of first and second time-bond sites was due to particles introduced during handling and relatively low sample size.

To evaluate whether blade-based die removal method damages the substrate wafer bond surface, we assessed the yield of the bottom daisy chain located 260 µm from the blade engagement side. The rebonded sites showed zero yield loss for this bottom chain (Table 1), indicating that the blade process did not damage the substrate wafer surface or underlying interconnects in this region.

TABLE 1. Yield for Blade Removal Method

	First round bond sites	Second round bond sites	Rebond sites
% Void-Free Yield from CSAM	93%	85%	94%
Main Chain % Electrical Yield	88%	88%	97%
Bottom Chain % Electrical Yield	93%	100%	100%

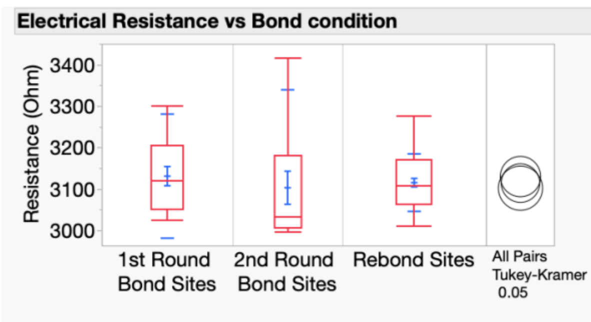

Fig. 9 Electrical resistance data of various bond groups for blade-based die removal approach

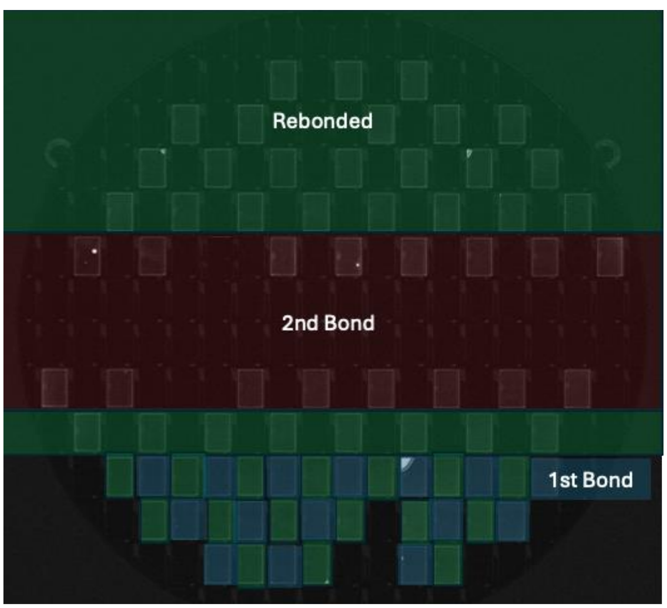

Fig. 10 CSAM image and various bond groups for blade-based die removal approach

Optical microscope inspection performed after the debond clean and prior to rebonding of debonded sites did not reveal any scratches or particles within the die footprint. However, a characteristic scratch just outside the die footprint was observed on the side opposite the edge on which the blade was engaged. Fig 11 shows an image of this defect. Since these superficial scratches were outside the die footprint, they did not result in any voiding or electrical yield loss.

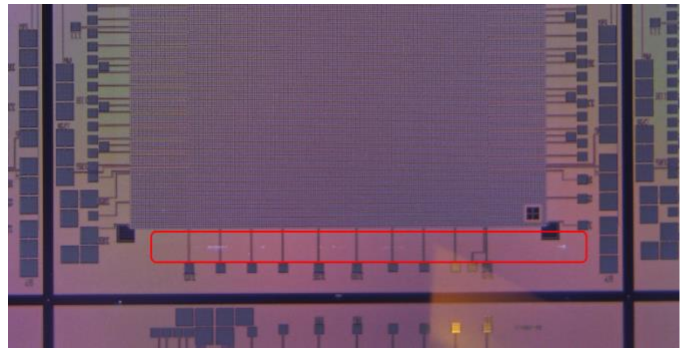

Fig. 11 Scratch defect incurred by blade-based die removal outside the die footprint

D. Debond/Rebond with adhesive-based pull method

The yield data for the adhesive-based pull debond/rebond trails with the electric test vehicle are shown in Table 2. The void and electrical yield data for the rebonded sites are comparable to those of the first and second round bond sites. Fig. 12 shows that the main-chain resistance values are comparable between rebonded and first and second round bond sites, indicating no measurable degradation of interconnect continuity from the debond/rebond process.

TABLE 2. Yield for Die Pull Method

	First round bond sites	Second round bond sites	Rebond sites
% Void-Free Yield from CSAM	98%	99%	98%
% Electrical Yield for Main chain	100%	98%	98%

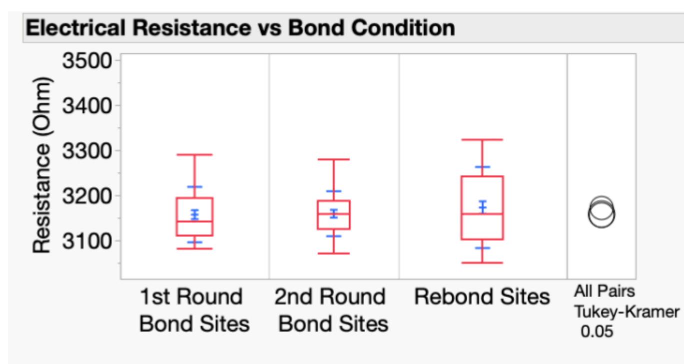

Fig. 12 Electrical resistance data of die pulled using die pull method

Fig. 13 shows the CSAM result of the various groups of dies bonded to the substrate. The CSAM image reveals that the voiding is similar across all three groups.

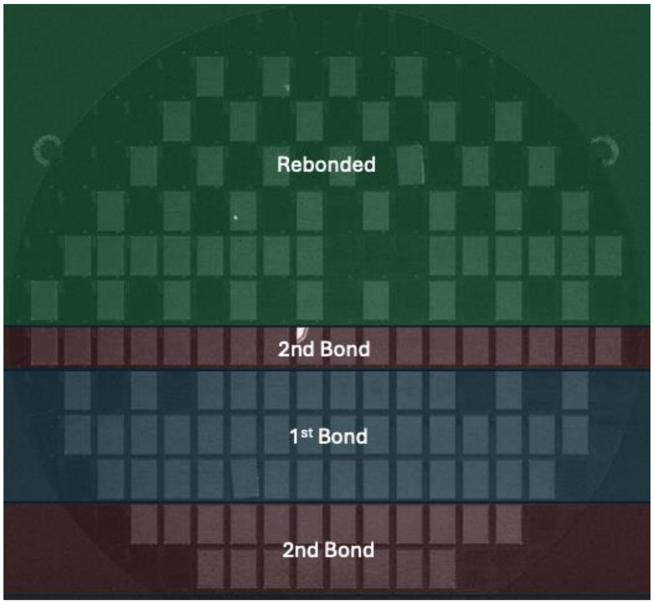

Fig. 13 CSAM image of various bond groups for adhesive-based die pull approach

Optical microscope inspection was performed after the debond clean and prior to rebonding of debonded sites. Unlike the blade debonded material, the pull debonded material did not show any scratches or particles anywhere in the die foot print or the surrounding area.

E. Effect of die thickness and die area on pull force

Figure 14 summarizes the effect of die thickness on required pull force for 8 x 12mm dies. Since initial trials with small stud areas in conjunction with the 50 µm dies occasionally resulted in either stud adhesion failure or die cracking, we increased the stud area, which prevented the dies from cracking. The results indicate no significant difference in pull force between the various die thicknesses.

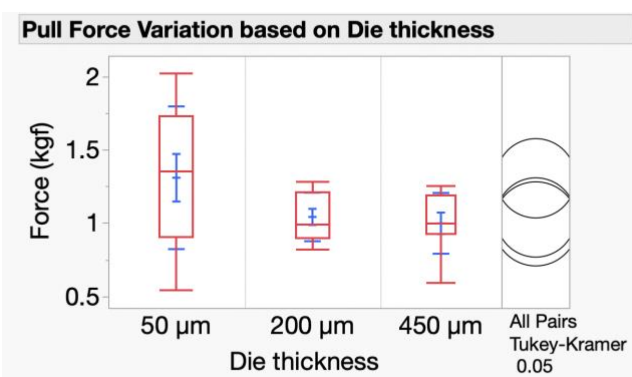

Fig. 14 Pull force versus die thickness (8x12 mm die)

Figure 15 shows the effect of die size on pull force with die thickness fixed at 200 µm. For 3×3 , 3.5×5.2 mm, and 8×12 mm dies, the pull force increased with increasing die size. For the three smallest die sizes, the required pull forces did not vary with stud position at center, edge, or corner of the die. Therefore, for operational simplicity, studs were placed at the die center for the smaller dies. However, for the largest dies (26 × 32mm, 200 µm), pulling using a center stud resulted in either stud adhesion failure or die cracking at extreme pull forces, whereas edge or corner stud placement enabled removal via an unzipping mechanism with pull forces comparable to those of 8 × 12 mm dies. Fig 16 shows a typical pull force versus time plot for a 26 x 32mm die showing the initial debond and subsequent unzipping of the die which correlated to the recorded video showing the propagation of the debonding front across the die.

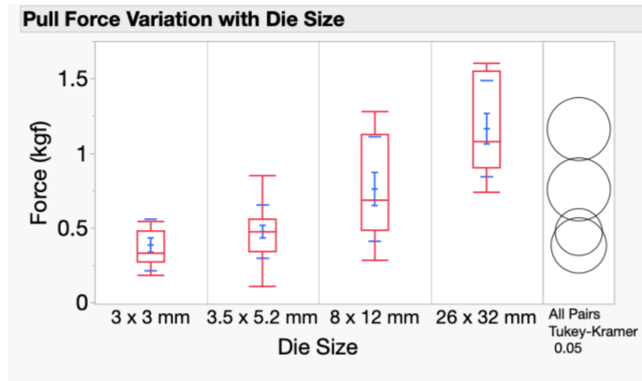

Fig. 15 Pull force versus die size (200 µm die thickness)

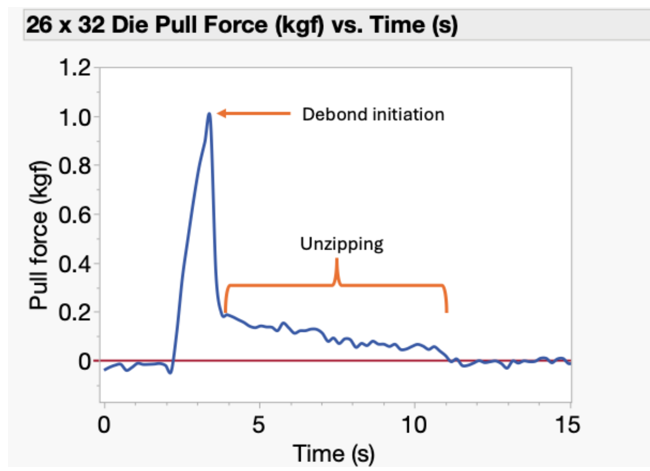

Fig. 16 Pull force profile of 26 x 32 mm die with stud attached to die corner

F. Die and substrate integrity

In all cases of die thickness and die size that were debonded, we were able to develop both a blade and pull debond process that resulted in no damage to the die. The only damage to the substrate was the pivot line scratch on the blade debonded sites as described earlier.

IV. ANALYSIS / DISCUSSION

A. Surface integrity and defects after debonding

Based on the AFM data and high-magnification microscopic inspection, debonding results in breaking the low energy dielectric to dielectric bonds at the bond interface without material transfer between the die and substrate.

Other than the benign scratch defect associated with the blade debond, there was no new defect mode observed. All yield loss in the rework trials was related to previously observed defect modes caused primarily by environmental particles due to manual handling in a Class 1000 (ISO 6) cleanroom. The debond process caused a small level of particle contamination of the substrate that was fully removed by the post-debond wet clean process. Due to the nature of the blade pressure on the side of the die, blade removal was more prone to particle generation compared to the pull debond method which involved no contact with the die edge.

B. *Storage temperature*

Storage at room temperature during the time between bonding and debonding resulted in an increasing bond energy that made debonding challenging after roughly seven days. Low-temperature storage (<0°C) significantly decreased the condensation reaction rate of the weak bonds at the interface, allowing the bond energy to remain low enough to easily debond after a month or longer from bonding.

C. *Mechanism of the debond*

As described in the results section, a characteristic scratch outside the footprint of dies removed by the blade debond method was observed. Slow motion video analysis shows that the blade induces die peeling that starts from the die edge in contact with the blade. The peel front then quickly moves across the die area to the opposite edge. This opposite edge then acts as a pivot point for the lifting die, and the induced pressure by the die edge results in the observed scratch in the substrate dielectric surface.

In the pull debond method, the force is directed straight upward from the interior of the die area. Therefore it might be assumed that the debond occurs simultaneous across the entire die area, which would result in a constant force per unit die area for the different die sizes. However, pull force versus die area data clearly shows a decreasing pull force per unit area as the die size increases as seen in Fig. 17.

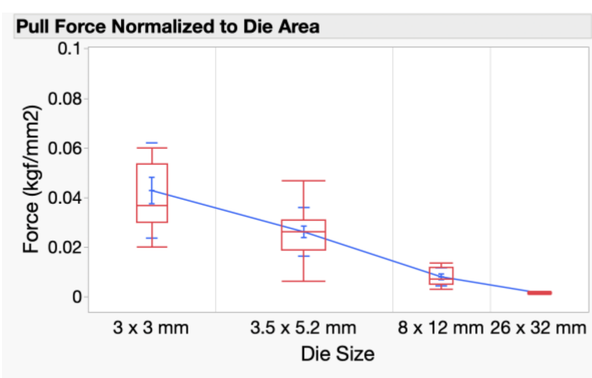

Fig. 17 Pull force/unit area for the different die sizes

This indicates an initial debonding of a region smaller than the full die foot print. This is in line with the unzipping phenomenon observed in 26 x 32 mm die upon pulling from the die corner (Fig. 16). Based on the high initial force needed to initiate the debonding followed by a lower force unzipping, it is likely that the initial debonding is of a finite area as opposed to the linear unzipping front that follows.

D. *Analysis of pull force versus die thickness*

Referring back to Fig. 14, the pull force versus die thickness is relatively constant. This is likely due to the fact that the stud used to remove the die covered a large fraction of the total die area, which was necessary to protect thin dies from cracking. By keeping the die rigid during debond process, we were able to pull thin dies with the same low pull force as thick dies.

E. *Analysis of pull force versus die size*

Referring back to Fig. 15, the required pull force increased slowly with die size and remained under 1.6 kgf even for the reticle maximum die size of 26x32 mm. The peak force is applied only momentarily until the debond front starts to propagate, and the pull force drops well below 0.5 kgf until the die is fully debonded. This force is not significantly higher than the downward force that is applied during hybrid bonding. No damage was detected on any die of any size or thickness that was pulled using an optimized debond process.

F. *Comparison of blade versus pull debond process*

Although both blade and pull methods are successful, each has its set of advantages and disadvantages that make one more beneficial than the other for different use cases.

Blade might be the better choice when the die size is small, there is need to minimize the debond force, and there is sufficient clearance to neighboring dies to insert a blade. Blade debonding is also the better choice when the debonded die can tolerate only a minimum clean between debond and rebond.

Pull debonding may be the better choice when cleanliness is critical, when dies are closely spaced, and when debonded die can tolerate adhesive removal from the die backside

V. Conclusion

Both blade and pull debond methods have been shown to successfully debond and allow rebonding to the debonded site without any yield loss penalty compared to the initially bonded structures. Debonding was performed on hybrid bonded material without modification of clean, activation, or bonding processes, and resulted in the same high bond energy after subsequent post bond anneal.

Rework can be performed successfully up to 7 days after bonding with storage at room temperature, and storage at -20ºC allows delays of a month or longer. Dies as thin as 50 µm can be easily removed with the use of a stud that covers a large fraction of the die area. Die up to reticle maximum size of 26 x 32 mm can be removed with a pull force of <1.6 kgf, which did not cause any detectable damage to die or substrate.

Based on the results of this initial trial, we see a clear path to refine these techniques for a high volume manufacturable D2W hybrid bond rework process.

Acknowledgment

The authors would like to thank Fraunhofer ASSID and L'Foundry for the fabrication of the electrical test vehicle.

REFERENCES

[1] S. Lhostis et al., "Reliable 300 mm Wafer Level Hybrid Bonding for 3D Stacked CMOS Image Sensors," 2016 IEEE 66th Electronic Components and Technology Conference (ECTC), Las Vegas, NV, USA, 2016, pp. 869-876, doi: 10.1109/ECTC.2016.202

[2] G. Gao *et al*., "Die to Wafer Stacking with Low Temperature Hybrid Bonding," *2020 IEEE 70th Electronic Components and Technology Conference (ECTC)*, Orlando, FL, USA, 2020, pp. 589-594, doi: 10.1109/ECTC32862.2020.00098.

[3] T. Workman et al., "Die to Wafer Hybrid Bonding and Fine Pitch Considerations," 2021 IEEE 71st Electronic Components and Technology Conference (ECTC), San Diego, CA, USA, 2021, pp. 2071-2077, doi: 10.1109/ECTC32696.2021.00326.

[4] G. Gao et al., "Die to Wafer Hybrid Bonding for Chiplet and Heterogeneous Integration: Die Size Effects Evaluation-Small Die Applications," 2022 IEEE 72nd Electronic Components and Technology Conference (ECTC), San Diego, CA, USA, 2022, pp. 1975-1981, doi: 10.1109/ECTC51906.2022.00310.

[5] G. Gao et al., “Surface Preparation Advances for Die Stacking with Hybrid Bonding” IMAPS Device Packaging Conference, Pheonix, AZ, March 3-6, 2025

[6] W. P. Maszara, G. Goetz, A. Caviglia, and J. B. McKitterick, "Bonding of silicon wafers for silicon‐on‐insulator," J. Appl. Phys. 64, 4943‐4950 (1988).